Progress In Electromagnetics Research, Vol. 144, 281–289, 2014

A Low-Cost Dual-Wideband Active GNSS Antenna with Low-Angle Multipath Mitigation for Vehicle Applications

Zhongbao Wang*, Hongmei Liu, Shaojun Fang, and Yuan Cao

Abstract—A low-cost dual-wideband active global navigation satellite system (GNSS) antenna is proposed for vehicle applications. An inverted shorted annular ring (ISAR) and a shorted annular ring (SAR) are used as radiation patches for low-angle multipath mitigation and operated respectively at 1164–1279 MHz and 1559–1610 MHz. To reduce the effect of the mutual coupling between the ISAR and SAR, meanwhile broaden the impedance bandwidth of the ISAR, defected ground structures are etched under the microstrip feed lines of the ISAR. Two trans-directional couplers are adopted to form orthogonal dual-feed networks of the ISAR and SAR for wideband circularly polarized reception. A combiner is adopted to merge two way signals into one way amplified by a wideband low noise amplifier with the proposed DC and RF collinear transmission technology. The experimental results show that the proposed antenna is better than the NovAtel GPS-703-GGG pinwheel antenna in terms of signal reception.

1. INTRODUCTION

Nowadays, global navigation satellite systems (GNSS) [1–3] are increasingly equipped on the vehicles such as aircrafts, ships and cars. For the GNSS antenna, it is usually mounted outboard and connected to the receiver inside the vehicle by a long coaxial cable (5–50 m) which causes a big insertion loss. Therefore, an active GNSS antenna includes a built-in low noise amplifier (LNA) which provides sufficient gain to overcome the coaxial cable loss while providing the proper signal level to the GNSS receiver is needed.

Several active patch antennas for global position system (GPS) applications have been reported. In 2000, an active GPS antenna was first realized with a single-feed circularly-polarized (CP) patch antenna and a single-stage 16-dB LNA [4]. Then, Q. Xue et al. introduced a two-stage 25-dB LNA to enhance the gain for automotive applications, but also used a single-feed CP patch antenna, which suffers from inherent narrow axial ratio (AR) bandwidth as a result of only operating at GPS L_1 band from 1573 to 1577 MHz [5]. To broaden the operation bandwidth, C.-S. Lee et al. adopted the dual-feed CP patch antenna and two LNA combined with a 3-dB coupler to realize an active GNSS antenna operating from 1530 to 1620 MHz [6]. Recently, with the development of GNSS, the requests for multi-frequency and multi-system navigation ability increase. To meet the needs, several dual-band active GNSS antennas have been developed by a few corporations such as NovAtel, Hemisphere, and Trimble. However, the design method of these antennas cannot be found in the literature and these antennas are very expensive (more than 1,600 U.S. dollars). Therefore, a low-cost dual-band active GNSS antenna is highly desired.

Furthermore, for high-precision GNSS applications, the required specifications of the receiving antenna are an AR lower than 3 dB and a pattern amplitude roll off of at least 10 dB from zenith to horizon to avoid the effects of multipath signals. To simultaneously meet these requirements, several

Received 12 December 2013, Accepted 22 January 2014, Scheduled 29 January 2014

* Corresponding author: Zhongbao Wang (wangzb@dlmu.edu.cn).

The authors are with the School of Information Science and Technology, Dalian Maritime University Dalian, Liaoning 116026, China.

low multipath GPS antennas have been proposed in the past including patch elements placed on the choke rings [7], pinwheel antennas [8], and reduced surface wave (RSW) antennas [9–12]. However, choke rings are usually bulky. Therefore, the RSW method is a better solution.

RSW antennas that belong to a class of patch radiators are designed with shorted annular ring (SAR) or inverted shorted annular ring (ISAR) patches. In [13, 14], single-band (L_1) GPS antennas based on the RSW concept were designed and shown to provide comparable multipath performance to the choke ring and pinwheel antennas. While a dual-band GPS antenna operating at the L_1 (1575 MHz) and L_2 (1227 MHz) frequencies has been designed by L. Boccia et al. using stacked SAR patches [15] and L. I. Basilio et al. combining a SAR patch an a ISAR patch [16]. In this paper, the focus is to broaden the bandwidth of the SAR and ISAR antennas and realize a low-cost dual-wideband active GNSS antenna with low-angle multipath mitigation for vehicle applications, which is compatible with GPS, GLONASS, Galileo and Compass systems.

2. ANTENNA DESIGN PROCEDURES

The desired GNSS antenna has the following specifications:

1) operating frequency range of 1164–1279 MHz and 1559–1610 MHz including all the GNSS operating frequencies,
2) right-hand circularly-polarized (RHCP) reception with passive gain larger than 5 dBi at zenith with a gain roll off of at least 10 dB from zenith to horizon,
3) LNA gain larger than 25 dB with noise figure less than 2 dB,
4) input DC voltage from +4.5 to +18.0 V, and
5) single feed matched with 50-Ω coaxial cable while DC input and RF output transmitted collinearly.

To meet the requirements, an active GNSS antenna is designed and analyzed with Ansoft HFSS EM simulation and Agilent ADS circuit simulation. The design concepts and procedures are organized as follows.

2.1. SAR and ISAR Design

Figure 1 shows the configuration of the proposed dual-feed CP antenna with the SAR and ISAR patches, which are printed on the upper side of the lower F4B substrate with a dielectric constant of 2.65, loss tangent of 0.001, and thickness of $H_2 = 3.0$ mm. An air gap is used in this configuration to achieve broader bandwidth, higher gain, and lower cost. However, thicker air gap implies longer feed probes with consequently more inductance leading to poor impedance matching. Therefore, instead of the direct probe feed in [16], the proximity-coupled feeds [1] with rectangle patches are used to introduce

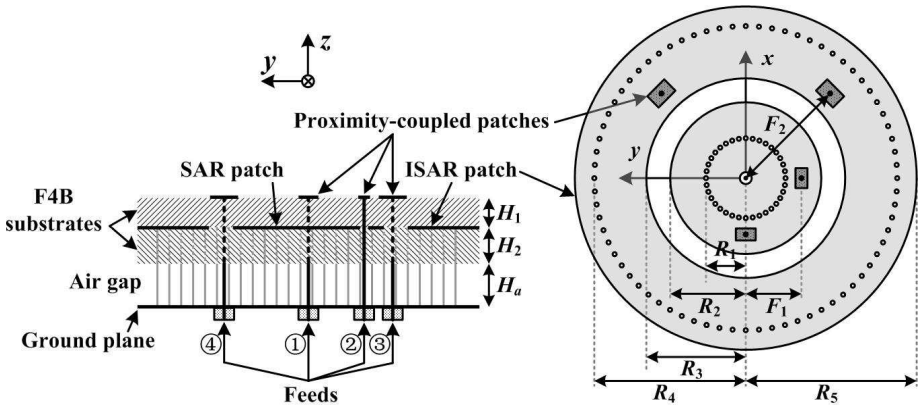

(a) Side view (b) Top view

Figure 1. Geometry of the proposed dual-feed circularly-polarized SAR and ISAR patch antennas.

capacitance that compensates for the increased inductance due to the longer probe. Proximity-coupled rectangle patches are located above the SAR and ISAR patches and are printed on the top side of the upper F4B substrate with thickness of $H_1 = 1.0\,\text{mm}$. The dimensions of the rectangle patches for exciting the SAR and ISAR patches are $2.6\,\text{mm} \times 10\,\text{mm}$ and $6.5\,\text{mm} \times 9\,\text{mm}$, respectively. For this design, the short-circuited boundary condition is implemented using an array of circular vias that form a connection between the patch conductor and the ground plane. To achieve CP reception, each of the SAR and ISAR patches is excited by utilizing an orthogonal dual-feed arrangement.

Figure 2(a) shows input matching of the dual-feed ISAR and SAR with $R_1 = 26.5\,\text{mm}$, $R_2 = 55.7\,\text{mm}$, $R_3 = 74.0\,\text{mm}$, $R_4 = 129.0\,\text{mm}$, $R_5 = 140.0\,\text{mm}$, $F_1 = 35.0\,\text{mm}$, $F_2 = 103.0\,\text{mm}$, and $H_a = 6.0\,\text{mm}$. It is found that by using the proximity-coupled feeds, the ISAR and SAR antennas have good impedance matching at 1200 MHz and 1575 MHz, respectively. However, higher resonant frequency of the ISAR antenna is near the operating frequency of the SAR antenna and the mutual coupling between the ISAR and SAR is greater than $-10\,\text{dB}$ as shown in Figure 3(a), which will increase the design complexity of the orthogonal dual-feed network. To solve the problem, defected ground structures (DGS) are etched under the microstrip feed lines of the ISAR as shown in Figure 4. After adopted the DGS with $d_1 = 5.8\,\text{mm}$, $d_2 = 5.8\,\text{mm}$, $d_3 = 2.7\,\text{mm}$, $d_4 = 24.6\,\text{mm}$, $d_5 = 0.4\,\text{mm}$, the mutual coupling between the ISAR and SAR is less than $-18\,\text{dB}$ at 1575 MHz as shown in Figure 3(b) and the impedance bandwidth of the ISAR with return loss greater than 10 dB is broadened as shown in Figure 2(b).

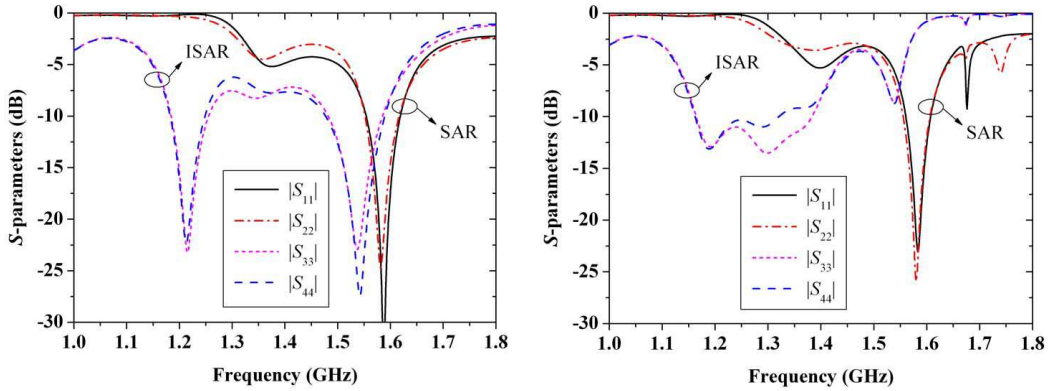

(a) Without DGS (b) With DGS

Figure 2. Simulated input matching of the dual-feed SAR and ISAR patch antennas.

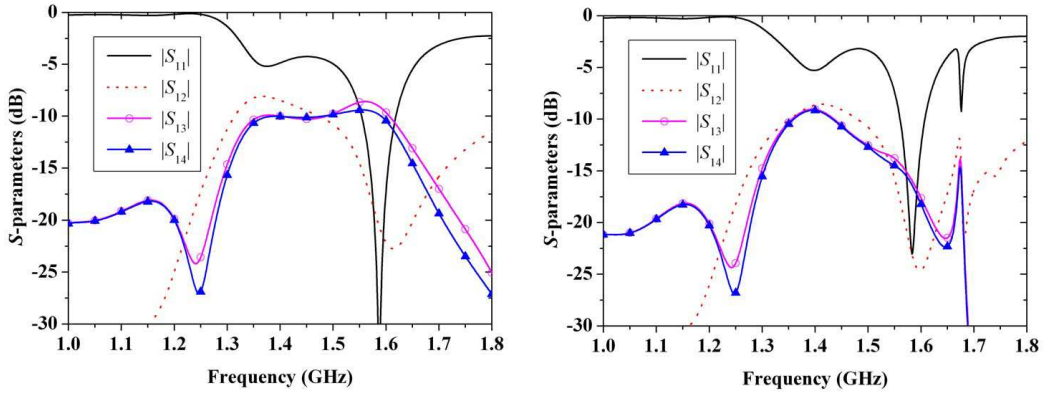

(a) Without DGS (b) With DGS

Figure 3. Simulated mutual coupling between the SAR and ISAR patch antennas.

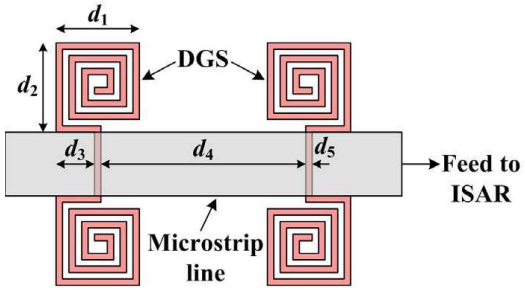

Figure 4. Geometry of the DGS etched under the microstrip feed lines of the ISAR.

2.2. Feed Network Design

Figure 5 shows the proposed feed network for the SAR and ISAR patch antennas. It is composed of a combiner, two TRD couplers and four DGS at the output ports of lower-band TRD coupler, which is designed and fabricated on the F4B substrate with the a thickness of 1.5 mm. To obtain tight coupling, TRD couplers with capacitor-loaded coupled lines are used to respectively feed the SAR and ISAR antennas. Based the theory analysis of the TRD coupler [17] and the number of the loaded capacitors is chosen to be 3, the capacitances of the loaded capacitors are $C_1 = 2.2\,\text{pF}$ and $C_2 = 3.0\,\text{pF}$ for lower- and upper-band TRD couplers, respectively. Meanwhile, the even- and odd-mode characteristic impedance of the coupled line are $Z_{0e} = 120.9\,\Omega$ and $Z_{0o} = 77.2\,\Omega$ for both TRD couplers with the port impedance of $Z_0 = 50\,\Omega$.

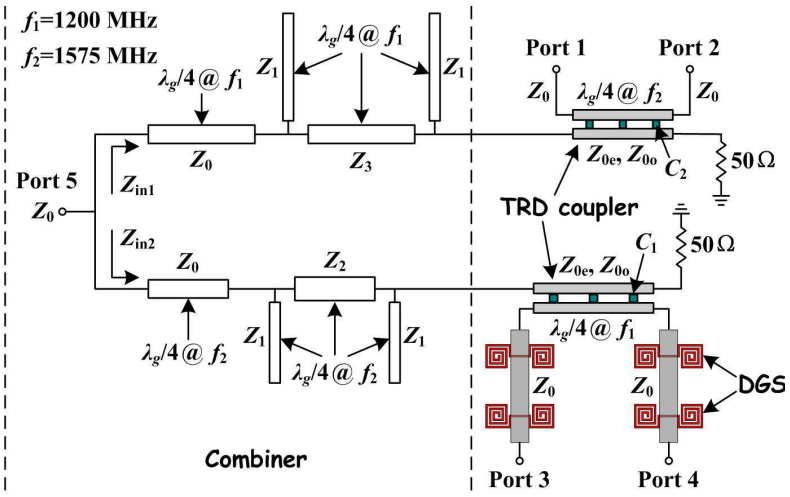

Figure 5. Schematic of the proposed feed network.

Furthermore, a combiner is used to merge lower- and upper-band GNSS signals into one way, and then amplified by a wideband LNA. The combiner consists of four $\lambda_g/4$ open-circuit lines and four $\lambda_g/4$ impedance transformers. Two $\lambda_g/4$ open-circuit lines connected by a $\lambda_g/4$ impedance transformer with respect to f_1 (or f_2) are used to realize a filter with stop-band centre frequency at f_1 (or f_2). The $\lambda_g/4$ impedance transformers are adopted as match circuits for $Z_{in1} = \infty$ and $Z_{in2} = Z_0$ at f_1, $Z_{in1} = Z_0$ and $Z_{in1} = \infty$ at f_2. Based on the match conditions, the line characteristic impedances of the combiner are $Z_1 = 90\,\Omega$, $Z_2 = 51\,\Omega$, and $Z_3 = 40\,\Omega$. Then using a transmission-line calculator such as *TX-LINE* or *LineCalc*, the dimensions of the microstrip lines and coupled lines can be easily obtained. So these parameters are not given here for conciseness.

In Figure 6 is shown the simulated and measured response of the feed network of the proposed feed network included the amplitude and phase responses. It is seen from the measured results that the proposed feed network delivered balanced output ports power distribution (amplitude difference less

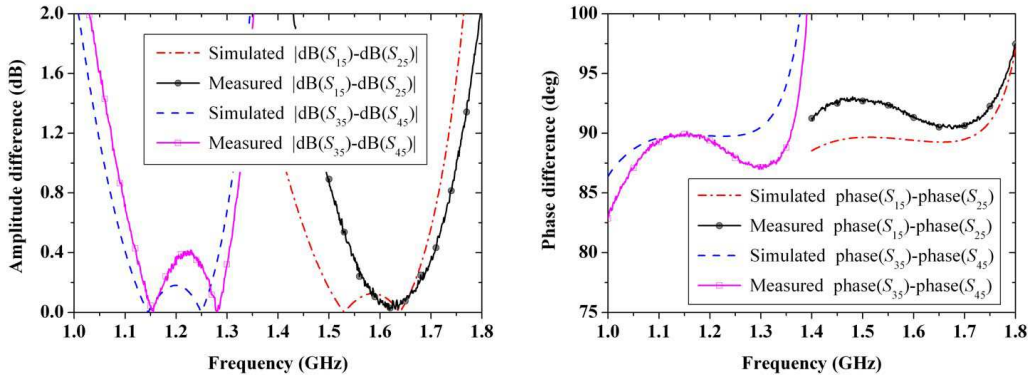

(a) Amplitude difference of the output ports (b) Phase difference of the output ports

Figure 6. Simulated and measured performances of the proposed feed network.

than 0.4 dB) and consistent 90° (±3°) output ports phase difference between port 1 and port 2 from 1544 to 1706 MHz and between port 3 and port 4 from 1122 to 1303 MHz.

2.3. Wideband LNA Design

To achieve wideband high gain with low noise, a two-stage LNA is designed by using the field effect transistor of ATF-54143. Both transistors are biased at 3 V with the same biasing circuits, and the detailed parameters are optimized by using Agilent ADS simulator and given in Figure 7. To realize DC input and RF output transmitted on the same cable, a voltage stabilizing diode of MIC5200-5.0BS is inserted between the RF output port of the LNA and the DC input port of the biasing circuit. When the input voltage of MIC5200-5.0BS is from +2.5 to +26 V, the output voltage can be fixed at 5 V. It

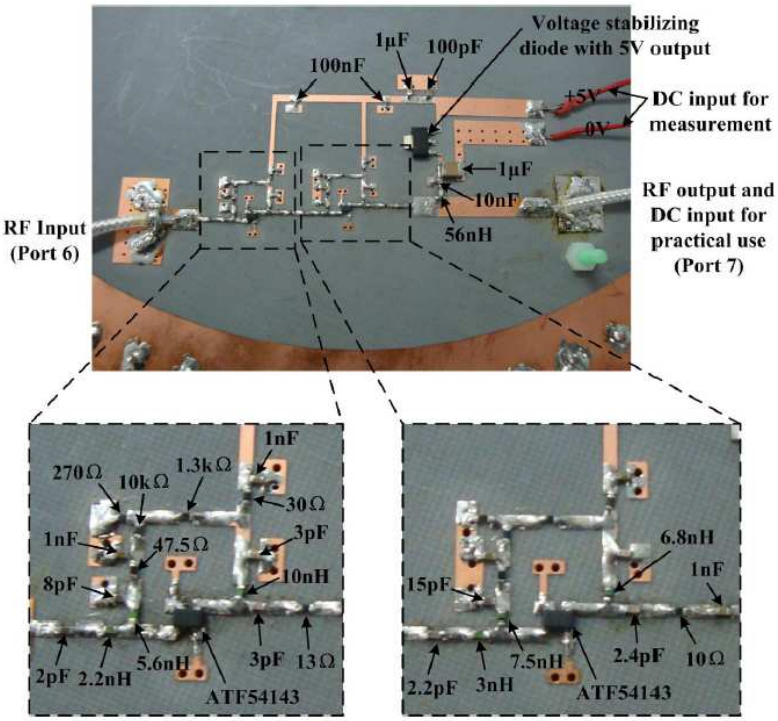

Figure 7. Photograph of the proposed two-stage LNA.

is noted that the DC input port shown in Figure 7 is only used to measure the performances of the LNA. In practical usage, the DC is fed from the port 7. Furthermore, the series inductor with 56 nH and shunt capacitors with 10 nF and 1 μF are used to block the RF signal into the voltage stabilizing diode.

Figure 8 gives the simulated and measured performances of the proposed two-stage LNA. It is observed from the measured results that the RF input VSWR (port 6) is less than 1.8, the RF output VSWR (port 7) is less than 1.4, the gain is more than 27.6 dB, and noise figure is 1.5 ± 0.3 dB from 1100 to 1660 MHz.

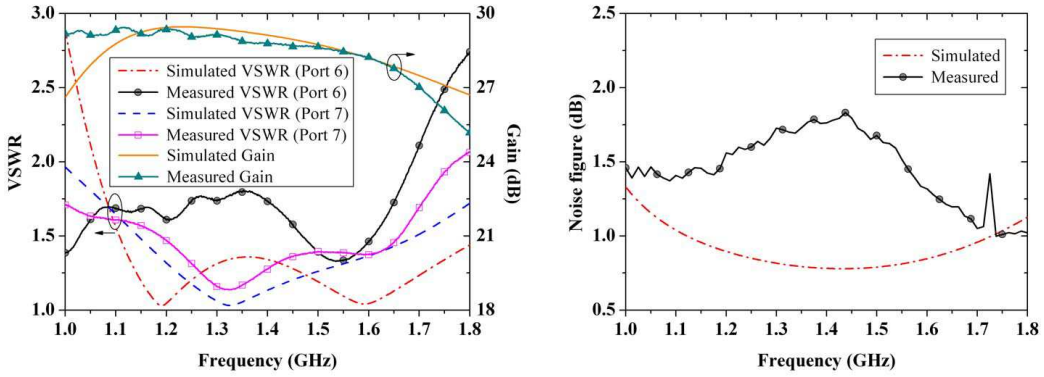

(a) VSWR and gain (b) Noise figure

Figure 8. Simulated and measured performances of the proposed LNA.

2.4. Antenna Integration with Feed Network and LNA

Figure 9 shows the fabricated prototype of the proposed active GNSS antenna. The ground of the feed network with DGS shown in Figure 9(a) is also used as the ground plane for the SAR and ISAR antennas. The air gap shown in Figure 1(a) is realized by using nine cylindrical plastic spacers with the length of 6 mm and the diameter of 5 mm. To obtain a satisfactory stability, all the copper-clad F4B laminates and plastic spacers are screwed together. Furthermore, the feed network and wideband LNA are fabricated on the same F4B laminates and connected with the SMA connector and coaxial cables when antenna practical use. The diameter of the ground plane is 280 mm.

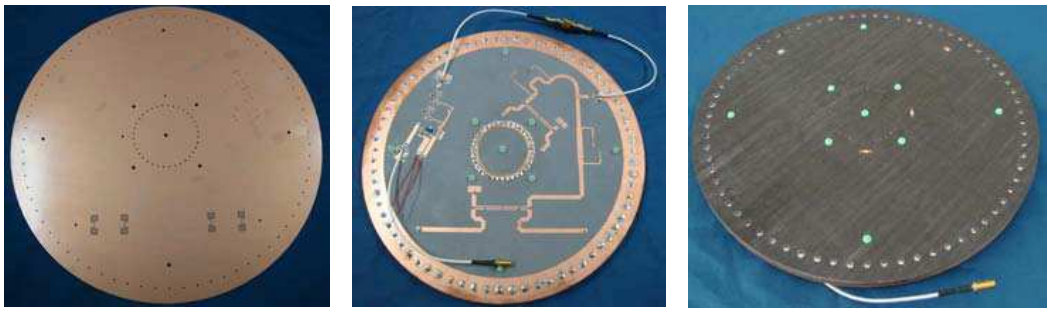

(a) Ground with DGS (b) Bottom view of antenna (c) Top view of antenna

Figure 9. Fabricated prototype of the proposed active GNSS antenna.

3. EXPERIMENTAL RESULTS AND ANALYSIS

A prototype was tested in an anechoic chamber. Figure 10(a) shows the simulated and measured VSWR of the passive GNSS antenna. The measured VSWR is less than 2.0 over the frequency range

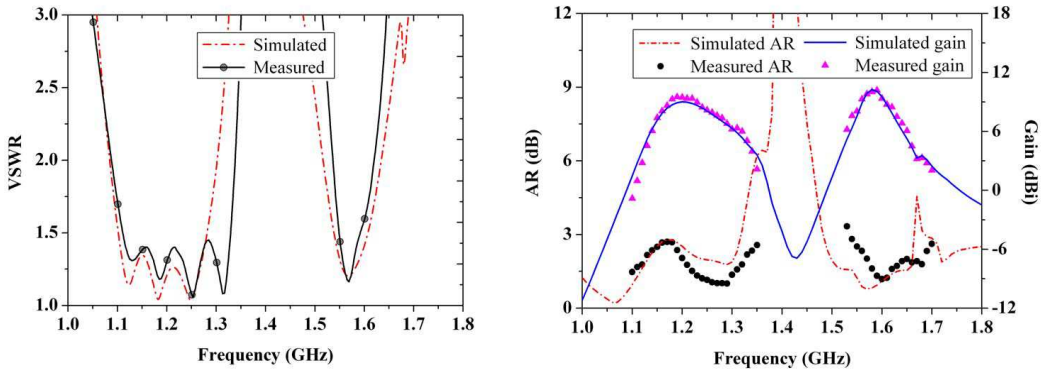

(a) VSWR (b) AR and Gain

Figure 10. Simulated and measured performances of the passive GNSS antenna.

of 1087–1337 MHz and 1536–1618 MHz. For all the GNSS operating frequencies at 1164–1279 MHz and 1559–1610 MHz, the VSWR is less than 1.5, which attribute to the use of the proposed feed network. A comparison between the simulated and measured AR in the zenith direction ($\theta = 0°$) is shown in Figure 10(b). The measured AR is less than 3 dB for all the GNSS operating frequencies. The simulated and measured gain is also shown in Figure 10(b). The antenna has a measured gain-level more than 7.3 dBi across the GNSS operating bands. When the proposed LNA is used, the antenna gain can be enhanced to be more than 36 dBi.

Figure 11 shows the simulated and measured radiation patterns at 1200 and 1575 MHz, having good agreement between the simulated and measured results. The measured RHCP fields are stronger than the left-hand circularly-polarized (LHCP) fields by more than 18 dB in the zenith direction ($\theta = 0°$). Furthermore, there is a gain roll off of 18 dB from zenith to horizon at 1200 MHz and that of 23 dB at 1575 MHz, which implies that the proposed antenna has an ability to reject low-angle multipath interference [18–20].

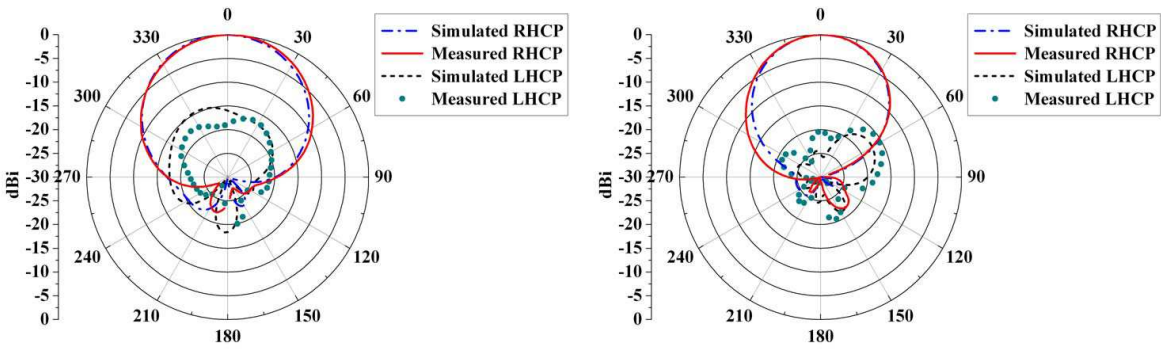

(a) 1200 MHz (b) 1575 MHz

Figure 11. Simulated and measured radiation pattern of the proposed GNSS antenna.

4. VALIDATION IN GNSS SYSTEM

To verify the operation of the proposed active antenna in GNSS system practical applications, the positioning measurements were carried out on one roof in a sunny day, and a NovAtel GPS-703-GGG pinwheel antenna is used for comparison. In the experiment, the proposed antenna and the GPS-703-GGG antenna are connected to a NovAtel GNSS receiver (FLEXPAK-V2-L1L2), which can be track GPS and GLONASS satellites and decode the GPS L_1 and L_2 signals for positioning. The performance

(a) Proposed antenna

(b) NovAtel GPS-703-GGG pinwheel antenna

Figure 12. Performance comparison between the proposed antenna and GPS-703-GGG antenna.

comparison between the proposed antenna and GPS-703-GGG antenna is given in Figure 12. It is seen from the constellation diagram of Figure 12(a) that the proposed antenna can track eight GPS satellites and seven GLONASS satellites. From the GPS tracking channel status window of Figure 12(a), the signal noise ratio (SNR) of all the L_1 and L_2 received signals is greater than 35 dB and that of eight signals is greater than 45 dB, which implies that the proposed LNA can amplify the weak GNSS signals and induce low noise. For the same one satellite, the SNR at L_1 and L_2 bands have smaller differences than the GPS-703-GGG antenna. Furthermore, it is found from the precision window in Figure 12 that the latitude and longitude errors for the proposed antenna are 1.82 m and 1.51 m, respectively, and that for GPS-703-GGG antenna are 2.04 m and 1.83 m. Therefore, the performance of the proposed antenna is better than that of the GPS-703-GGG antenna.

5. CONCLUSIONS

A novel dual-wideband active GNSS antenna with DC and RF collinear transmission technology for vehicle applications is designed, fabricated and experimentally tested. The experimental results show that at all the GNSS operating frequencies, the VSWR of the proposed antenna is less than 1.5, the AR is less than 3 dB, the passive gain is greater than 7.3 dBi with active gain of more than 36 dBi, and the gain roll off from zenith to horizon is more than 18 dB. The proposed antenna can operate in GPS, GLONASS, Galileo and Compass systems with high gain and multipath rejection capabilities [18–20]. Furthermore, the antenna is validated in a practical GNSS system and the signal reception performance and cost are superior to the NovAtel GPS-703-GGG pinwheel antenna. Therefore, the proposed antenna can be a good candidate for high-precision GNSS applications.

ACKNOWLEDGMENT

This work was supported jointly by the Traffic Applied Basic Research Project of the Ministry of Transport of China (No. 2010-329-225-030), Scientific Research Project of the Department of Education of Liaoning Province (No. L2013196), Fundamental Research Funds for the Central Universities

(No. 3132013053), National Natural Science Foundation of China (No. 61231006), and National Key Technologies R&D Program of China (No. 2012BAH36B01).

REFERENCES

1. Wang, Z. B., S. J. Fang, S. Q. Fu, and S. W. Lü, "Dual-band probe-fed stacked patch antenna for GNSS applications," *IEEE Antennas Wireless Propag. Lett.*, Vol. 8, 100–103, 2009.
2. Li, D., P. F. Guo, Q. Dai, and Y. Q. Fu, "Broadband capacitively coupled stacked patch antenna for GNSS applications," *IEEE Antennas Wireless Propag. Lett.*, Vol. 11, 701–704, 2012.
3. Li, X., L. Yang, and Q. Chen, "Novel design of stacked dual layer strip lines fed wideband patch antenna for GNSS application," *Progress In Electromagnetics Research C*, Vol. 35, 193–203, 2013.
4. Thiagarajah, S., B. M. Ali, and M. H. Habaebi, "Circular polarized active microstrip antenna for commercial GPS application," *Proceedings of TENCON 2000*, 109–114, Kuala Lumpur, Malaysia, 2000.
5. Xue, Q., H. Wong, K. M. Shum, K. M. Luk, and C. H. Chan, "Active receiving antennas for automotive applications," *Proceedings of IEEE Antennas and Propagation Society International Symposium*, 1443–1446, Monterey, USA, 2004.
6. Lee, C.-S., C.-I. Hsu, M.-L. Her, and D.-C. Chang, "The design and implementation of a GPS active microstrip antenna," *Journal of Da-Yeh University*, Vol. 12, No. 1, 49–56, 2003.
7. Wang, E. C., Z. P. Wang, and Z. Chang, "A wideband antenna for global navigation satellite system with reduced multipath effect," *IEEE Antennas Wireless Propag. Lett.*, Vol. 12, 124–127, 2013.
8. Kunysz, W., "High performance GPS pinwheel antenna," Novatel Inc., 2000, Available: http://www.novatel.com/assets/Documents/Papers/gps_pinwheel_ant.pdf.
9. Jackson, D. R., J. T. Williams, A. K. Bhattacharyya, R. L. Smith, S. J. Buchheit, and S. A. Long, "Microstrip patch designs that do not excite surface waves," *IEEE Trans. Antennas Propag.*, Vol. 41, No. 8, 1026–1037, 1993.
10. Boccia, L., G. Amendola, and G. Di Massa, "A shorted elliptical patch antenna for GPS applications," *IEEE Antennas Wireless Propag. Lett.*, Vol. 2, 6–8, 2003.
11. Amendola, G., L. Boccia, and G. Di Massa, "Shorted elliptical patch antennas with reduced surface waves on two frequency bands," *IEEE Trans. Antennas Propag.*, Vol. 53, No. 6, 1946–1956, 2005.
12. Basilio, L. I., J. T. Williams, D. R. Jackson, and R. L. Chen, "Characteristics of an inverted shorted annular-ring-reduced surface-wave antenna," *IEEE Antennas Wireless Propag. Lett.*, Vol. 7, 123–126, 2008.
13. Boccia, L., G. Amendola, G. Di Massa, and L. Giulicchi, "Shorted annular patch antennas for multipath rejection in GPS-based attitude determination systems," *Microw. Opt. Technol. Lett.*, Vol. 28, No. 1, 47–51, 2001.
14. Basilio, L. I., J. T. Williams, D. R. Jackson, and M. A. Khayat, "A comparative study for a new GPS reduced-surface-wave antenna," *IEEE Antennas Wireless Propag. Lett.*, Vol. 4, 233–236, 2005.
15. Boccia, L., G. Amendola, and G. Di Massa, "A dual frequency microstrip patch antenna for high-precision GPS applications," *IEEE Antennas Wireless Propag. Lett.*, Vol. 3, 157–160, 2004.
16. Basilio, L. I., R. L. Chen, J. T. Williams, and D. R. Jackson, "A new planar dual-band GPS antenna designed for reduced susceptibility to low-angle multipath," *IEEE Trans. Antennas Propag.*, Vol. 55, No. 8, 2358–2366, 2007.
17. Shie, C. I., J. C. Cheng, and S. C. Chou, "Transdirectional coupled-line couplers implemented by periodical shunt capacitors," *IEEE Trans. Microw. Theory Tech.*, Vol. 57, No. 12, 2981–1988, 2009.
18. Boccia, L., G. Amendola, and G. Di Massa, "Performance evaluation of shorted annular patch antennas for high-precision GPS systems," *IET Microw. Antennas Propag.*, Vol. 1, 465–471, 2007.
19. Boccia, L., G. Amendola, S. Gao, and C. C. Chen, "Quantitative evaluation of multipath rejection capabilities of GNSS antennas," *GPS Solutions*, 2013, DOI 10.1007/s10291-013-0321-0.
20. Rao, B. R., W. Kunysz, R. Fante, and K. McDonald, *GPS/GNSS Antennas*, Artech House, 2012.